Physics of the Earth and Planetary Interiors 175 (2009) 137–144

Contents lists available at ScienceDirect

Physics of the Earth and Planetary Interiors

journal homepage: www.elsevier.com/locate/pepi

Melting in the deep upper mantle oceanward of the Honshu slab

Brian Bagley[a,*], Anna M. Courtier[b], Justin Revenaugh[a]

[a] Department of Geology and Geophysics, University of Minnesota, 310 Pillsbury Drive SE, Minneapolis, MN 55455, USA
[b] Department of Geology and Environmental Science, James Madison University, 800 S. Main Street, MSC 6903, Harrisonburg, VA 22807, USA

ARTICLE INFO

Article history:
Received 14 May 2008
Received in revised form 10 March 2009
Accepted 10 March 2009

Keywords:
Mantle
Transition zone
Discontinuities
Partial melting
Water
Low-velocity zone

ABSTRACT

We examine the upper mantle and transition zone beneath the western Pacific using multiple ScS reverberations. A low-velocity zone (LVZ) is found above the 410-km discontinuity oceanward of the subducting Honshu slab at an average depth of 356 km, with a thickness that ranges from 50 to 75 km assuming the LVZ continues to the 410-km discontinuity, which is locally elevated. The low-velocity region is evident in previous tomographic studies, and our results suggest that the anomaly is best explained by a layer of partial melt. The layer may be entrained from above by subduction or produced in situ by the combined effects of water and temperature. A self-consistent model that explains local P-wave velocities (Obayashi, M., Sugioka, H., Yoshimitsu, J., Fukao, Y., 2006. High temperature anomalies oceanward of subducting slabs at the 410-km discontinuity. Earth and Planetary Science Letters 243, 149–158) and our observations calls for a maximum temperature anomaly of ~150 °C and a resulting maximum olivine water content after melting of 0.100 wt. %.

1. Introduction

Seismic observations of a low-velocity zone (LVZ) directly above the mantle transition zone are becoming more frequent with increasingly high-resolution studies of the upper mantle. Revenaugh and Sipkin (1994) made the first observation of a LVZ in the deep upper mantle beneath eastern China and the Sea of Japan using multiple ScS reverberations. They suggested that the LVZ was a layer of negatively buoyant melt resting atop the 410-km discontinuity. Since then, similar explanations have been invoked to account for observations in a variety of geologic settings. Most of these study areas are located above subducting slabs (Revenaugh and Sipkin, 1994; Pino and Helmberger, 1997; Song et al., 2004; Gao et al., 2006; Courtier and Revenaugh, 2007), and the observations are most commonly attributed to regions of water-induced partial melting above the transition zone.

Similar observations exist in other geologic settings as well. Most recently, Vinnik and Farra (2007) found a LVZ with an average depth of 350 km at numerous continental locations in Asia, Africa, and Antarctica using S-wave receiver functions. Vinnik and Farra (2002), Vinnik et al. (2003), and Vinnik and Farra (2007) associate the LVZ with areas of continental flood basalts and also relate the feature to a local change in the hydration state of the mantle.

A LVZ oceanward of subduction has been found in many P- and S-wave tomographic studies (e.g., Bijwaard et al., 1998; Fukao et al., 2001; Zhao, 2004; Obayashi et al., 2006). The LVZ oceanward of the Honshu slab imaged by P- and S-wave tomography has been attributed to hot upwelling due to local-scale convection or a rising mantle plume (Zhao, 2004). Obayashi et al. (2006) used triplicated P-waves to establish the first non-tomographic observation of this LVZ. Their P-wave velocity models and waveform analysis indicate that the layer is ~50 km thick and is also associated with a temperature increase of 200 °C. An explanation requiring both increased temperature and either anomalously high iron or water content was put forward by the authors. Their model also requires a velocity decrease near the 410-km discontinuity and a depression of the 410-km discontinuity on the order of 10's of kilometers. The mechanism proposed for producing the melt layer is a hydrous, hot upwelling that melts during phase transformation to olivine, with the resulting melt then entrained toward the subducting slab. In this scenario the Petit-spot (Hirano et al., 2001; Fujiwara et al., 2007) is assumed to be the surface expression of this activity. The location of this LVZ makes the combined analysis of P-wave tomography, triplicated P-waves (Obayashi et al., 2006), and multiple ScS reverberations (this study) ideal.

Water-induced melting, resulting from the combination of high water content in the transition zone and the lower water storage capacity of minerals in the upper mantle, is usually invoked to explain the presence of a LVZ in the deep upper mantle. The transition zone is a potential reservoir for water due to the enhanced water storage capacity of the transition zone minerals, wadsleyite and ringwoodite, over that of upper and lower mantle mineral assemblages (e.g., Kohlstedt et al., 1996; Hirschmann et al., 2005; Bolfan-Casanova et al., 2005, 2000; Murakami et al., 2002). The

* Corresponding author. Tel.: +1 612 624 8557; fax: +1 612 625 3819.
E-mail address: bagl0025@umn.edu (B. Bagley).

0031-9201/$ – see front matter © 2009 Elsevier B.V. All rights reserved.
doi:10.1016/j.pepi.2009.03.007

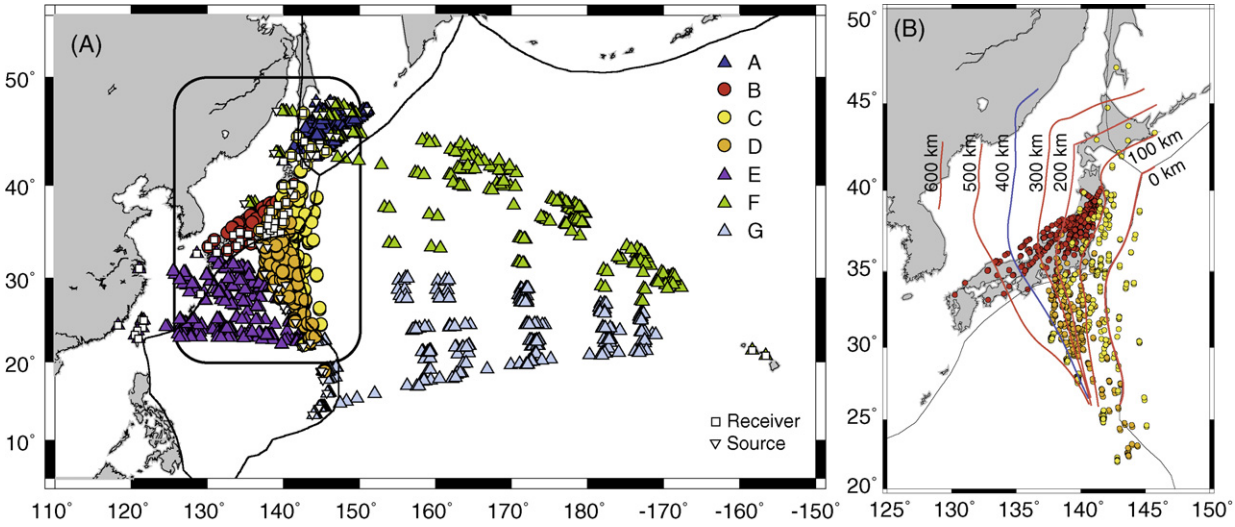

Fig. 1. A: Multiple ScS surface bounce points for the seven paths in this study. Circles indicate paths where melt was inferred (Paths B–D). Triangles indicate paths were no melt was required (Paths A, E, F, and G). B: ScS surface bounce points for Paths B–D with depth contours for the subducting slab (Niu et al., 2005). Source (squares) and receivers (inverted triangles) are also shown; the exact coordinates for the sources can be found in Table 1. Note that all of these paths sample the region oceanward of the slab at depths up to 410 km.

effects of variations in water content and water storage capacity in the transition zone and overlying upper mantle have been topics of recent debate (Bercovici and Karato, 2003; Hirschmann et al., 2006a; Leahy and Bercovici, 2007). If the water content of material upwelling from the transition zone exceeds the local storage capacity of the overlying upper mantle, melting will occur (Hirschmann et al., 2005). Hirschmann et al. (2006a) suggested that the melt layer would have a maximum thickness of ~7 km, unless the water storage capacity of the upper mantle continued to diminish toward the surface, in which case melt would persist all the way to the surface. The transition zone water filter hypothesis (Bercovici and Karato, 2003; Karato et al., 2006; Leahy and Bercovici, 2007) predicts a laterally extensive, possibly global, melt layer above the 410-km discontinuity varying in thickness from 3 m (Leahy and Bercovici, 2007) to 10 km (Bercovici and Karato, 2003). All of these thickness estimates are at odds with layer thicknesses of the seismic observations of LVZs atop the 410-km discontinuity. Seismic studies generally describe the thickness of the melt layer as the distance from the top of the LVZ to the top of the 410-km discontinuity. S-wave triplication and ScS reverberation methods yield melt layer thicknesses that range from ~20 (Song et al., 2004) to 100 km thick (Revenaugh and Sipkin, 1994).

Possible mechanisms for producing a layer of partial melt thicker than that predicted by petrologic and geodynamic studies are discussed in Courtier and Revenaugh (2007). If olivine above the transition zone is under-saturated with water, and the storage capacity declines with decreasing depth, then the onset of melting

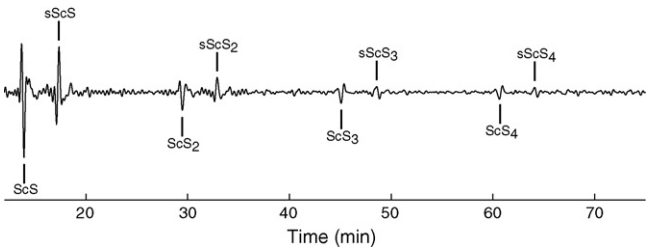

Fig. 2. Long-period, SH-polarized seismogram from the October 3, 2001 earthquake (47.080°N, 148.630°E, 280 km depth) recorded at station URH (42.930°N, 143.671°E) with multiple ScS phases within the reverberative interval labeled. Reflections from the transition zone discontinuities are prominent in the intervals between multiple ScS pairs.

would occur at shallower depths (Courtier and Revenaugh, 2007). The resulting melt may be negatively buoyant (Matsukage et al., 2005; Sakamaki et al., 2006) and would percolate down toward the 410-km discontinuity, creating a thick LVZ. Additional debate exists regarding the dynamics of the melt layer itself. Due to the flux balance that occurs between diffuse upwelling and localized downwelling in subduction zones, Bercovici and Karato (2003), Karato et al. (2006), and Leahy and Bercovici (2007) predict that negatively buoyant melt would eventually sink or become entrained by slabs and assimilated back into the transition zone. This effectively creates a scenario where water is sequestered in the transition zone, which may be problematic considering the balance required between the exosphere and the Earth's internal water budget. If this balance is not maintained, a decrease in eustatic sea level might occur during periods of increased subduction (for a review see Hirschmann, 2006b), although this would presumably be balanced, at least in part, by lower mean oceanic lithosphere age and reduced bathymetry.

Honda et al. (2007) also propose a scenario whereby slab entrainment is responsible for the localization of hot material atop the transition zone. In this scenario, anomalously hot material is transported from nearby regions within the shallow upper mantle towards the subduction zone and downward. Further entrainment of the material is kinetically inhibited by the 410-km discontinuity, which causes the melt to pool in the deep upper mantle. This model does not consider the effects of water.

If the seismically observed LVZ above the transition zone is caused by water-induced melting above the 410-km discontinuity, there must be a mechanism to introduce water to the region. Irifune et al. (1998) and Shieh et al. (1998) showed that dense hydrous magnesium silicates (DHMS) present in subducting slabs transition into superhydrous phase B and phase D at transition zone and mid-mantle pressures. These phases and water stored in nominally anhydrous minerals (e.g., Kohlstedt et al., 1996; Katayama and Nakashima, 2003) may introduce water into the transition zone and possibly the deep mantle (in the case of DHMS) within subduction complexes. However, while this provides a source of mantle water on the arc side of the slab, it does not introduce significant amounts of water to the mantle below the subducting plate.

Variability in discontinuity depths can help to discern whether temperature or water is a cause of the anomalous observations above the 410-km discontinuity. Due to the Clapeyron slopes of

Table 1
Discontinuity depths [z (km)] and reflection coefficients [$R(z)$ (%)] from preferred synthetic reflectivity profiles. Bandpass filter parameters provided are low cut, low corner, high corner, and high cut in mHz. TZ = Transition Zone. The errors associated with the LVZ reflection coefficients for paths containing melt were calculated using a jackknife method. See Fig. 1 for path locations.

Path	Filter	Hales z, $R(z)$	Gutenberg z, $R(z)$	Lehmann z, $R(z)$	X z, $R(z)$	Melt z, $R(z)$	410 z, $R(z)$	Mid TZ z, $R(z)$	660 z, $R(z)$
A	8 10 45 60	60, 8.9					426, 3.6		663, 4.5
B	8 10 45 60	66, 5.4				359, -2.0 ± 0.8	409, 3.2		649, 2.4
C	8 10 45 60	53, 9.0		218, 3.0		364, -1.9 ± 0.6	422, 2.6	514, 2.1	667, 2.5
D	8 10 45 60	52, 6.4		214, 1.6		343, -1.0 ± 0.9	416, 4.3		675, 5.1
E	8 10 45 60			239, 4.0			422, 3.0	485, 2.8 581, 1.7	674, 4.7
F	15 17 40 60		83, −5.2		332, 2.3		423, 3.3		660, 5.0
G	12 14 40 60		89, −4.9		299, 1.5		426, 2.5		666, 3.6

the olivine components in the upper mantle, high temperatures would cause the 410-km discontinuity to deepen (e.g., Katsura et al., 2004a), while the 660-km discontinuity would occur at a shallower depth (e.g., Katsura et al., 2003). Water present as hydrogen in point defects in mineral structures affects the transition zone discontinuities as well. The behavior predicted at 410 km depth is attributed to the stabilization of wadsleyite in the presence of water. Wood (1995) and Smyth and Frost (2002) predict that the 410-km discontinuity will broaden and migrate to a shallower depth in response to a hydrous, but undersaturated, transition zone. Chen et al. (2002) predicts that the 410-km discontinuity will sharpen and migrate to a shallower depth if the region is saturated with water. The 660-km discontinuity is also affected by the presence of water and may deepen (Higo et al., 2001). The competing effects of water and temperature on discontinuity structure, as well as the additional presence of carbon, or varying amounts of iron, can make the changes in transition zone discontinuity depths difficult to interpret.

We re-examine the region sampled by Obayashi et al. (2006) whose combination of regional P-wave tomography and P-

Table 2
Source parameters for the earthquakes used in this study. Paths using each event are listed in the last column. Letters refer to Fig. 1.

Date	Origin time (UTC)	Latitude (°)	Longitude (°)	Depth (km)	m_b	Paths
March 31, 1995	14:01:41	38.15	135.06	365	6.2	F
April 8, 1995	17:45:13	21.83	142.69	267	6.7	G
August 23, 1995	07:06:03	18.86	145.22	595	7.1	G
August 24, 1995	06:28:55	18.85	145.12	602	5.8	G
August 24, 1995	07:54:43	18.82	145.04	612	6.1	G
October 20, 1995	19:21:29	18.71	145.54	225	6.1	G
February 1, 1996	07:18:04	44.85	146.27	170	6.2	F
February 14, 1996	21:26:56	29.25	140.45	141	6.0	G
February 22, 1996	14:59:09	45.26	148.54	124	6.3	A,F
March 16, 1996	22:04:06	28.98	138.94	477	6.7	C,D,E
June 26, 1996	03:22:03	27.73	139.75	468	6.3	C,D
July 6, 1996	21:36:29	21.97	142.83	241	6.2	C,G
July 15, 1996	16:51:22	18.73	145.63	176	6.3	C,D,E,G
December 22, 1996	14:53:28	43.21	138.92	226	6.5	F
April 23, 1997	19:44:28	13.99	144.90	101	6.5	G
November 15, 1997	07:05:17	43.81	145.02	161	6.1	A,F
February 7, 1998	01:13:37	24.79	141.75	525	5.9	C,D
February 7, 1998	01:19:00	24.83	141.75	525	6.4	C,E
February 28, 1998	17:38:49	33.46	138.12	291	5.7	B
May 15, 1998	05:58:06	14.18	144.88	154	6.1	G
September 8, 1998	09:10:03	13.26	144.01	141	6.1	G
January 12, 1999	02:32:26	26.74	140.17	440	6.0	G
May 12, 1999	17:59:22	43.03	143.84	102	6.5	F
July 3, 1999	05:30:10	26.32	140.48	430	6.1	G
February 15, 2000	02:05:01	17.68	145.40	522	5.9	G
March 28, 2000	11:00:23	22.34	143.73	126	7.6	D,E,G
June 9, 2000	22:35:14	30.47	137.68	472	5.8	C,D
June 9, 2000	23:31:45	30.49	137.73	485	6.3	C,E
June 21, 2000	16:25:06	14.11	144.96	112	5.9	G
July 10, 2000	09:58:19	46.83	145.42	360	6.1	F
August 6, 2000	07:27:13	28.86	139.56	395	7.4	G
October 27, 2000	04:21:52	26.27	140.46	388	6.3	G
December 22, 2000	10:13:01	44.79	147.20	140	6.3	A,F
February 26, 2001	05:58:22	46.82	144.53	392	6.1	F
October 3, 2001	17:25:13	47.08	148.63	285	5.9	A,F
December 2, 2001	13:01:54	39.40	141.09	123	6.5	B
June 3, 2002	09:15:01	27.56	139.78	488	5.9	C,D,E,G
November 17, 2002	04:53:54	47.82	146.21	459	7.3	F
November 17, 2002	04:53:48	47.95	146.42	470	5.8	A
July 27, 2003	06:25:32	47.15	139.25	470	6.8	A,F
November 12, 2003	08:26:46	33.63	137.02	391	6.4	F
July 8, 2004	10:30:49	47.20	151.30	128	6.4	A
November 7, 2004	02:02:26	47.95	144.48	474	6.2	A
February 2, 2005	02:30:26	14.08	144.72	159	6.3	G
February 5, 2005	03:34:26	16.01	145.87	143	6.6	G

waveform modeling was not able to determine the sharpness of the upper boundary of the LVZ on top of the 410-km discontinuity. Here we use multiple ScS reverberations, SH-polarized shear phases that are reflected off of the core-mantle boundary and discontinuities within the mantle. In addition to being more sensitive to changes in shear strength than compressional waves, multiple ScS reverberations require sharp (less than 15–20 km thick) changes in velocity and/or density, making them better suited for distinguishing between diffuse thermal anomalies and partial melt horizons.

2. Data

We conducted a study of the transition zone and upper mantle beneath the Philippine Sea and the Pacific Ocean (Fig. 1A). We collected all archived broadband and long-period seismic records of nearby events with magnitude (m_b) ≥ 5.7 and hypocentral depths greater than 80 km. These seismograms (e.g., Fig. 2) were rotated, deconvolved to ground velocity, and decimated to a 3-s sampling interval following Revenaugh and Jordan (1989). A cosine-squared zero-phase bandpass filter was applied; filter parameters are listed in Table 1. Each seismogram was visually inspected, and those with low signal-to-noise ratios or apparent source complexity were discarded from the dataset. We additionally excluded events with source depths between 300 and 450 km in the near-subduction paths to ensure that potential observations of a LVZ above the 410-km discontinuity are not the result of misinterpreted depth phases.

The resulting dataset includes 45 events that occurred between 1995 and 2005, with depths (z) of $101 \leq z \leq 612$ km, and magnitudes of $5.7 \leq m_b \leq 7.6$ (Table 2). These data were divided into seven source–receiver paths that contain between 12 and 32 seismograms each. The seismic corridors were selected to discretely sample the arc and oceanward side of the slabs located along the western edge of the Pacific plate with as little geologic overlap as possible, paying close attention the geography of the low-velocity anomaly identified by Obayashi et al. (2006).

3. Method

We use the inversion/migration method of Revenaugh and Jordan (1991a,b) to extract mantle layering information from zeroth- and first-order multiple ScS reverberations. First order top- and bottom-side ScS_n ($n = 1$–4) reflections from 410 km for paths containing a LVZ above the 410-km discontinuity are shown in Fig. 3. The migration folds information from both top- and bottom-side reflections from mantle discontinuities into a 1D depth profile (e.g., Fig. 4) of radial normal-incidence shear-wave reflection coefficient (one half of the shear-wave impedance contrast). It is relatively insensitive to along-path velocity heterogeneity, which imposes a small downward bias in estimated reflection coefficient magnitude.

Synthetic seismograms are computed and migrated in the same manner as the data to produce model profiles. Discontinuities are added to the initially smooth background model to match data profiles. We add as few discontinuities as necessary to obtain an accurate match, relying in part on previous modeling and nearby paths for guidance in selecting reflector ensembles. Occasionally, ghost discontinuities arise from the partial chance correlation of reverberations related to multiple ScS and those from multiple sScS from different discontinuities. These ghost discontinuities can have reflectivity peaks that exceed the 95% confidence level but are well matched in a synthetic model without introducing a discontinuity into the velocity model. Estimated reflector depths are corrected to PREM (Dziewonski and Anderson, 1981) using a waveform inversion derived crustal model, digital bathymetry/topography of the free surface, and 3D velocity variability, following Revenaugh and Jordan (1991b).

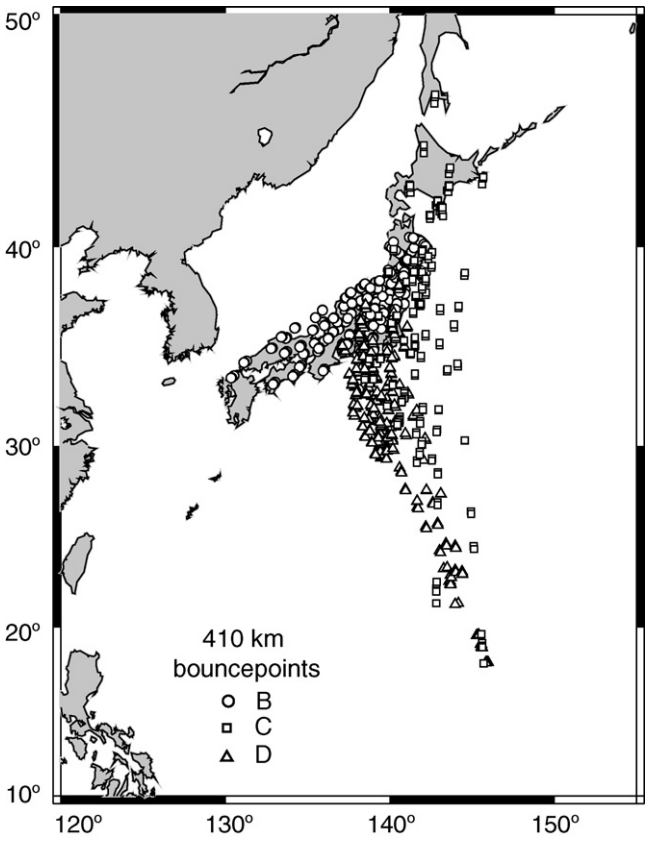

Fig. 3. First order top- and bottom-side ScS_n ($n = 1$–4) reflections from 410 km for paths containing a LVZ above the 410-km discontinuity. Individual Paths (B–D) are indicated with a circle, square, and triangle, respectively.

4. Results

Reflectivity profiles for all paths in the study are shown in Fig. 4; the corresponding depths and impedance contrasts can be found in Table 1. The Hales discontinuity (see Revenaugh and Jordan (1991c) for discontinuity nomenclature) is found in all of the paths except Paths E, F and G, and depths of the observations range between 52 and 66 km. The Gutenberg discontinuity is found beneath the island of Honshu (Path B) at a depth of 99 km, and in the ocean-crossing Paths (F and G) at depths of 83 and 89 km, respectively. The Lehmann discontinuity is found in all three paths originating from the Izu Bonin trench (Paths C–E) and varies in depth between 214 and 239 km. There is evidence of the X discontinuity in both of the ocean-crossing corridors (Paths F and G). All of the paths contain the 410- and 660-km discontinuities. Paths C and E contain evidence of the 520-km discontinuity, with the discontinuity split in the latter path. Paths B–D are modeled best by additionally placing a LVZ above the 410-km discontinuity, with a thickness (δ) that ranges from $50 \leq \delta \leq 75$ km (Fig. 4A). In all cases, a discontinuity is modeled in the synthetic only when it is required to match the data profile. The inclusion of the discontinuity in our model indicates that the match between data and synthetic profiles improved upon the addition of the discontinuity. Ghost discontinuities that are matched in the synthetic without the addition of a discontinuity at the depth in the synthetic are not indicative of true mantle structure. To cast aside any doubt concerning whether the LVZs we model are real or ghost features, we have included synthetic profiles with and without the LVZ in Fig. 4A. This clearly shows that the addition of the LVZ to the velocity model is required to match the data profiles. Fig. 4B is an example of two Paths (A and E) that appear to have an LVZ in the data profile. However, modeling this

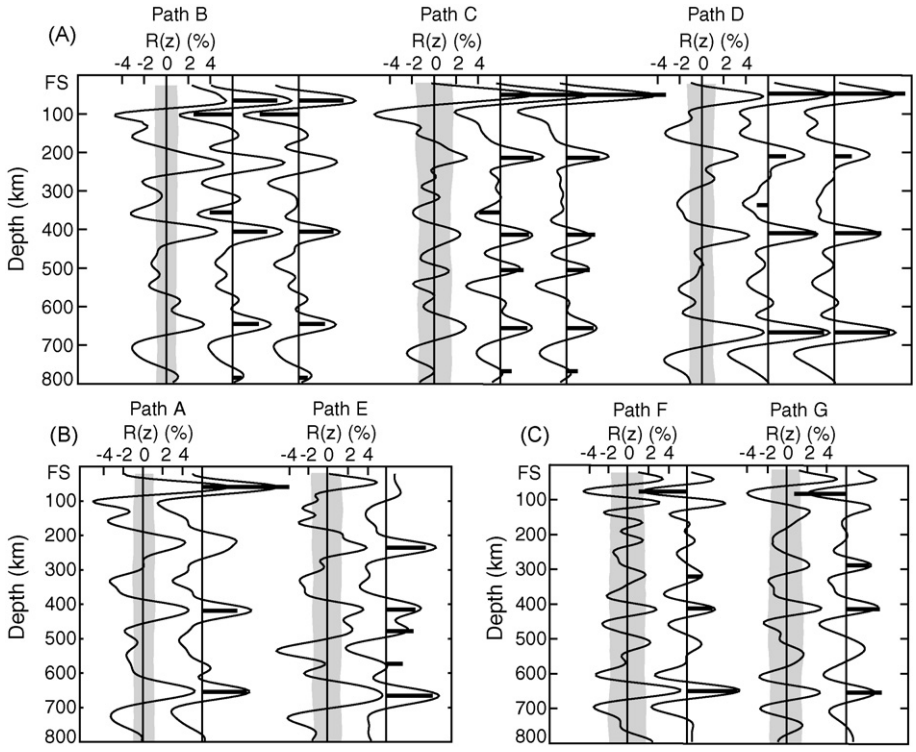

Fig. 4. SH reflectivity profiles. $R(z)$ (%) with depth from the free surface (FS) to 800 km. The gray bands displayed with data profiles represent the 95% confidence interval for incoherent colored noise. The magnitude of the reflection coefficients listed in Table 1 are shown as horizontal bars. See Fig. 1 for path locations and the text for a discussion of peaks exceeding the gray bands that are not modeled with a discontinuity. A: Reflectivity profiles for the three source–receiver Paths (B–D) requiring a LVZ atop the transition zone. For each path, data are shown on the left, synthetic data from the preferred model containing the LVZ is shown in the middle, and synthetic data from a model containing no LVZ are shown on the right. B: Data (left) and synthetic (right) reflectivity profiles for the two Paths (A and E) adjacent to the paths containing melt. C: Data (left) and synthetic (right) reflectivity profiles for the two ocean-crossing Paths (F and G).

feature is not required to obtain a good match between the data and synthetic profiles, and this feature is therefore considered a ghost discontinuity in these paths. We find no significant depression or uplift of either the 410- or 660-km discontinuities between paths. We also observe discontinuities in the mid-mantle, which are outside the scope of this paper.

5. Discussion

Our paths sample the region studied by Obayashi et al. (2006) as closely as allowed by the differing source–receiver geometries required by the two different methods. The region where Obayashi et al. (2006) observed the LVZ is well sampled by our data and our results are similar to theirs, with the exception of the region directly east of Taiwan. We sample this region in Path E and see no evidence of a LVZ, whereas they report a localized LVZ between the Ryuku and Izu-Bonin trenches. Path E covers a broad geographic area compared to the extent of the anomaly observed by Obayashi et al. (2006), so its absence in our data may be a result of the lateral averaging that occurs along our source–receiver path. Fig. 1B shows the geographic location of the three Paths (B–D) containing evidence of a LVZ overlaid by contours marking the depth of the slab (Niu et al., 2005). All three paths clearly sample the mantle oceanward of the slab at 410 km depth, although completely avoiding interaction with the slab is not possible. However, arrivals due to the slab (an inclined feature) would not stack coherently across the collection of top- and bottom-side reverberations with varying numbers of core reflections and differing sources. The LVZ we observe must be due to a sub-horizontal feature present above the 410-km discontinuity.

The thickness (δ) of the melt layer we observe is on the same order as that used by Obayashi et al. (2006) in their model. As previously discussed, none of the geodynamic (Bercovici and Karato, 2003; Leahy and Bercovici, 2007; Karato et al., 2006) or petrologic (Hirschmann et al., 2006a) studies offer a mechanism to explain a melt layer this thick, but these studies assume that the material upwelling from the transition zone is saturated as it passes through the 410-km discontinuity, and melts immediately. If, however, the upwelling material is water-rich but not saturated at 410 km depth, it may not melt until it reaches saturation at shallower depths in the upper mantle (e.g., Courtier and Revenaugh, 2007). If melting occurs near 350 km, the melt will be near the density crossover with ambient mantle rocks (Agee and Walker, 1993; Ohtani et al., 1995). If water content varies, some melts may be buoyant and others dense, helping to explain both the LVZ at depth and the surface volcanism of the overlying Petit-spot (Fujiwara et al., 2007). The resulting melt that remains sequestered in the deep upper mantle may have a zero degree dihedral angle (Cmiral et al., 1998; Yoshino et al., 2007), and the signature of melt in the surrounding mantle may be preserved due to surface tension (Hier-Majumder et al., 2006). This remnant signature of melt could explain the apparent melt thickness observed seismically and may enable seismic detection at lower melt-fractions since thin melt films are highly effective at reducing shear modulus (e.g., Walsh, 1969).

The depth of the 410-km discontinuity changes in a predictable manner in response to changes in temperature and/or water. Tradeoffs in the response of the 410-km discontinuity to slab uplift and increased temperature or water content outside the slab exist and make interpretation of discontinuity depths difficult. Warmer temperatures should cause the 410-km discontinuity to deepen, whereas colder temperatures have the opposite effect (Katsura et al., 2004a). Increased water content should cause the 410-km discontinuity to broaden and migrate to shallower depths (Wood, 1995; Helffrich and Wood, 1996; Smyth and Frost, 2002). Although

the depth variations we observe between paths are small, the three paths sampling the LVZ have the shallowest 410-km discontinuity depths (Table 1). This limits the temperature excess in the region and suggests the importance of water in creating the partial melt layer.

Dry peridotite does not melt until ~2100 °C at 350 km depth (Zhang and Herzberg, 1994). For an average mantle potential temperature of 1350 °C (e.g., Courtier et al., 2007), the corresponding temperature at 350 km depth is 1445 °C (Katsura et al., 2004b). Under these conditions a temperature anomaly of 655 °C is required to induce melting due solely to temperature. Such a large temperature anomaly is not indicated by tomography (Obayashi et al., 2006) or by our estimates of discontinuity depth, which would be sensitive to a depression of the magnitude predicted by such a temperature anomaly despite horizontal averaging.

Recent high-pressure studies of olivine (Smyth et al., 2006; Litasov et al., 2007) provide a method for estimating water content in the pressure–temperature range of the LVZ we observe. The estimated maximum water content in olivine at 1445 °C in the presence of melt is ~0.229 wt. %. This value is below the water storage capacity of olivine without melt present (~0.394 wt. %; Hirschmann et al., 2005), but well above the normal water content of the average mid-ocean ridge basalt (MORB) (~0.011 wt. %; Workman and Hart, 2005). While the amount of water required to induce melting by hydration alone may be a reasonable water content on the arcside of a subducting slab, a mechanism for obtaining a comparable water content oceanward of the slab has not been suggested to date. Given the extremely high temperature anomaly or increased amount of water needed for melting to occur due to either temperature or water alone, we conclude that if the LVZ we observe is the result of in situ melting, it must be induced by the combined effects of temperature and water.

Obayashi et al. (2006) estimated a 200–250 °C temperature anomaly in the region based on P-wave velocity anomalies from 350 km to the top of the 410-km discontinuity. Under their hypothesis as well as ours, this is a region of partial melt, making it difficult to separate the velocity decrement due to temperature alone. The P-wave velocity anomalies they observe above the transition zone, as well as the depths and reflection coefficients for the LVZ in our preferred models are influenced by temperature and melt, therefore P-wave velocity anomalies occurring below the 410-km discontinuity, where there is likely no melt, provide a better proxy for temperature. Regional tomography (Obayashi et al., 2006) shows a maximum P-wave velocity anomaly of −0.6% near 500 km depth. This depth was chosen to reduce any effect of tomographic smearing from the anomaly above the transition zone. We estimate the corresponding temperature anomaly to be 155 °C, using the tomographic velocity anomaly and a value of 0.0039%/°C (Cammarano et al., 2003) to relate velocity deviation with temperature. The values from Cammarano et al. (2003) are based on a 1300 °C geotherm. We use an average mantle potential temperature of 1350 °C, therefore the 155 °C calculated using the 1300 °C geotherm and a P-wave velocity anomaly of −0.6% is an upper bound for the temperature anomaly in the study area. Since tomographic models are often blurred and may indicate velocity anomalies smaller than actual magnitude, we also compute the temperature anomaly associated with a 67% larger anomaly (P-wave velocity decrement of −1.0%) obtaining a temperature anomaly of 255 °C.

We estimate an upper bound for local water content as well. Including the 155 °C anomaly, the mantle potential temperature at 350 km is 1600 °C (Katsura et al., 2004b). Combining the results from Smyth et al. (2006) and Litasov et al. (2007) we estimate the maximum water content in olivine in this region to be ~0.100 wt. %. This value is for water content in olivine in the presence of melt and is therefore an estimate of the current water content in olivine, rather than the amount of water in olivine before melting occurred.

The ScS reverberation method is sensitive to sharp density and velocity contrasts; therefore a diffuse thermal anomaly is unlikely to produce a sufficient impedance contrast to cause observable higher order reflections. In our models, the top of the LVZ is marked by an impedance decrease of −1.0 to −2.0%. Partial melting has a larger effect on S-wave velocities than P-wave velocities, and the ratio dln Vs:dln Vp in the presence of partial melt at depths near 350 km is approximately 2.3:1 (Berryman, 2000). If we assume that density does not change across the top of the LVZ, then the impedance contrast we observe is due solely to changes in velocity. If density does change across the boundary, it would likely increase rather than decrease, making our calculation a minimum estimate. Obayashi et al. (2006) estimates the total P-wave velocity reduction due to temperature and melt to be 2.2%. To compare this with our S-wave velocity reduction ~350 km we need to subtract the P-wave velocity reduction due to temperature, which we take to be 0.6%, the velocity decrement in the presumably melt-free transition zone. Using 1.6% as the P-wave velocity reduction due solely to melt (Obayashi et al., 2006) we estimate an average dln Vs:dln Vp ratio of 2.0:1 across the three Paths (B–D) where the LVZ is located. Estimates for the individual paths vary from 1.3:1 to 2.5:1. Although there is considerable uncertainty in both the numerator and denominator, the results are at least consistent with predicted velocity ratios. Paths F and G, the two ocean-crossing paths, help to constrain the extent of the melt layer oceanward of Japan. The reflectivity profiles for these paths (Fig. 4C) show no evidence of melt above the 410-km discontinuity, indicating that the LVZ we observe is localized near the subduction zone (Fig. 1) and does not extend significantly out into the central Pacific.

This interpretation requires hot material upwelling from at least transition zone depths. Mantle material near the subduction zone is normally entrained by the slab and pulled downward. However, the slab under Japan is a flat-lying slab that does not penetrate the 660-km discontinuity (e.g., Van der Hilst et al., 1991; Fukao et al., 2001). This slab geometry is indicative of trench migration (Christensen, 1996, 2001; Olbertz et al., 1997), which may reduce downward entrainment, perhaps facilitating ascent of a hot upwelling through the transition zone.

Honda et al. (2007) propose that the velocity anomaly atop the 410-km discontinuity in the study area results from the entrainment of hot material originally located at a shallower depth, likely the remains of a former mantle plume. The anomalous material is entrained by the overlying plate and remains entrained as the plate is subducted. In their model, penetration of the 410-km discontinuity by the anomalous material is kinetically inhibited due to its higher temperature. The residence time of the anomaly above the transition zone is on the order of 100 Myr and depends on temperature and viscosity. However, as discussed previously, slab entrainment in the area may be weak due to the stalling of the slab within the transition zone. Additionally, unless melting occurs under water-rich conditions, a temperature anomaly equal to that predicted earlier for dry peridotite melting at 350 km depth would have to be present, which is not supported by topography of the 410-km discontinuity. For these reasons, we prefer the mechanism of in situ melting resulting from the combined effects of increased temperature and water content.

6. Conclusions

This region provides a unique source–receiver geometry, allowing analysis of mantle structure at transition zone depths using tomography, P-wave triplications, and ScS reverberations. LVZ anomalies also appear in the deep upper mantle near other subduction zones in tomographic models, indicating these may be a fairly common phenomena. Using an impedance-sensitive method that requires coherent reflections from discontinuities in the mantle, we

detect the same LVZ observed by Obayashi et al. (2006). One scenario they propose attributes the LVZ to a combination of increased temperature and a 50-km thick partial melt layer. Our results confirm that this is indeed a possibility and is more likely than other mechanisms that have been proposed, including increased iron content or purely thermal anomalies. If the LVZ were the result of melting due to either temperature or water alone, unrealistically high temperature or a mechanism for introducing large amounts water into the transition zone oceanward of subduction is required. We favor a simpler solution, attributing the melt layer to the combined effects of water and temperature, and estimate a maximum temperature anomaly of 155 °C and a resulting maximum olivine water content after melting of 0.100 wt. %. In our interpretation, melting occurs at the upper boundary of the LVZ, and some melt may escape upwards feeding Petit-spot volcanism. Additionally, the presence of melt should lower viscosity near the slab. This would result in less material being entrained by subduction and carried into the transition zone.

Acknowledgements

GMT software (Wessel and Smith, 1998) was used to prepare some of the figures. The Incorporated Research Institutions for Seismology (IRIS), Ocean Hemisphere Project (OHP), and F-Net supplied data. This research was supported by NSF grant EAR-0437424. Courtier benefited from a Doctoral Dissertation Fellowship at the University of Minnesota.

References

Agee, C.B., Walker, D., 1993. Olivine flotation in mantle melt. Earth and Planetary Science Letters 114, 315–324.
Bercovici, D., Karato, S., 2003. Whole-mantle convection and the transition-zone water filter. Nature (London) 425, 39–44.
Berryman, J.G., 2000. Seismic velocity decrement ratios for regions of partial melt in the lower mantle. Geophysical Research Letters 27, 421–424.
Bijwaard, H., Spakman, W., Engdahl, E.R., 1998. Closing the gap between regional and global travel time tomography. Journal of Geophysical Research 103, 30–130, 078.
Bolfan-Casanova, N., Keppler, H., Rubie, D.C., 2000. Water partitioning between nominally anhydrous minerals in the MgO–SiO_2–H_2O system up to 24 GPa; implications for the distribution of water in the Earth's mantle. Earth and Planetary Science Letters 182, 209–221.
Bolfan-Casanova, N., Kleppe, A.K., Welch, M.D., Wright, K., 2005. Water in the Earth's mantle; protons in minerals. Mineralogical Magazine 69, 229–257.
Cammarano, F., Goes, S., Vacher, P., Giardini, D., 2003. Inferring upper-mantle temperatures from seismic velocities. Physics of the Earth and Planetary Interiors 138, 197–222.
Chen, J., Inoue, T., Yurimoto, H., Weidner, D.J., 2002. Effect of water on olivine-wadsleyite phase boundary in the $(Mg, Fe)_2SiO_4$ system. Geophysical Research Letters 29, 4.
Christensen, U.R., 1996. The influence of trench migration on slab penetration into the lower mantle. Earth Planet Science Letters 140, 27–39.
Christensen, U.R., 2001. Geodynamic models of deep subduction. Physics of the Earth and Planetary Interiors 127, 25–34.
Cmiral, M., Fitz Gerald, J.D., Faul, U.H., Green, D.H., 1998. A close look at dihedral angles and melt geometry in olivine-basalt aggregates; a TEM study. Contributions to Mineralogy and Petrology 130, 336–345.
Courtier, A.M., Revenaugh, J., 2007. Deep upper-mantle melting beneath the Tasman and Coral Seas detected with multiple ScS reverberations. Earth and Planetary Science Letters 259, 66–76.
Courtier, A.M., Jackson, M.G., Lawrence, J.F., Wang, Z., Lee, C.-T.A., Halama, R., Warren, J., Workman, R., Xu, W., Hirschmann, M.M., Larson, A.M., Hart, S.R., Stixrude, L., Lithgow-Bertelloni, C., Chen, W.-P., 2007. Correlation of seismic and petrologic thermometers suggests deep thermal anomalies beneath hotspots. Earth and Planetary Science Letters 264, 308–316.
Dziewonski, A.M., Anderson, D.L., 1981. Preliminary reference Earth model. Physics of the Earth and Planetary Interiors 25, 297–356.
Fujiwara, T., Hirano, N., Abe, N., Takizawa, K., 2007. Subsurface structure of the "petit-spot" volcanoes on the northwestern Pacific Plate. Geophysical Research Letters 34, L13305, doi:10.1029/2007GL030439.
Fukao, Y., Widiyantoro, S., Obayashi, M., 2001. Stagnant slabs in the upper and lower mantle transition region. Reviews of Geophysics 39, 291–323.
Gao, W., Matzel, E., Grand, S.P., 2006. Upper mantle seismic structure beneath eastern Mexico determined from P and S waveform inversion and its implications. Journal of Geophysical Research 111, B08307, doi:10.1029/2006JB004304.
Helffrich, G.R., Wood, B.J., 1996. 410 km Discontinuity sharpness and the form of the olivine alpha–beta phase diagram; resolution of apparent seismic contradictions. Geophysical Journal International 126, F7–F12.
Hier-Majumder, S., Ricard, Y., Bercovici, D., 2006. Role of grain boundaries in magma migration and storage. Earth and Planetary Science Letters 248, 735–749.
Higo, Y., Inoue, T., Irifune, T., Yurimoto, H., 2001. Effect of water on the spinel-postspinel transformation in Mg_2SiO_4. Geophysical Research Letters 28, 3505–3508.
Hirano, N., Kawamura, K., Hattori, M., Saito, K., Ogawa, Y., 2001. A new type of intraplate volcanism; young alkali-basalts discovered from the subducting Pacific Plate, northern Japan Trench. Geophysical Research Letters 28, 2719–2722.
Hirschmann, M.M., Aubaud, C., Withers, A.C., 2005. Storage capacity of H_2O in nominally anhydrous minerals in the upper mantle. Earth and Planetary Science Letters 236, 167–181.
Hirschmann, M.M., Withers, A.C., Aubaud, C., 2006a. Petrologic structure of a hydrous 410 km discontinuity. In: Jacobsen, S.D., Van der Lee, S. (Eds.), Earth's Deep Water Cycle. American Geophysical Union, pp. 277–287.
Hirschmann, M.M., 2006b. Water, melting, and the deep Earth H_2O cycle. Annual Review of Earth and Planetary Sciences 34, 629–653.
Honda, S., Morishige, M., Orihashi, Y., 2007. Sinking hot anomaly trapped at the 410 km discontinuity near the Honshu subduction zone, Japan. Earth and Planetary Science Letters 261, 565–577.
Irifune, T., Kubo, N., Isshiki, M., Yamasaki, Y., 1998. Phase transformations in serpentine and transportation of water into the lower mantle. Geophysical Research Letters 25, 203–206.
Karato, S.-., Bercovici, D., Leahy, G., Richard, G., Jing, Z., 2006. The transition-zone water filter model for global material circulation: where do we stand? In: Jacobsen, S.D., Van der Lee, S. (Eds.), Earth's Deep Water Cycle. American Geophysical Union, pp. 289–313.
Katayama, I., Nakashima, S., 2003. Hydroxyl in clinopyroxene from the deep subducted crust; evidence for H_2O transport into the mantle. American Mineralogist 88, 229–234.
Katsura, T., Yamada, H., Shinmei, T., Kubo, A., Ono, S., Kanzaki, M., Yoneda, A., Walter, M.J., Ito, E., Urakawa, S., Funakoshi, K., Utsumi, W., 2003. Post-spinel transition in Mg_2SiO_4 determined by high P-T in situ X-ray diffractometry; Phase transitions and mantle discontinuities. Physics of the Earth and Planetary Interiors 136, 11–24.
Katsura, T., Yokoshi, S., Song, M., Kawabe, K., Tsujimura, T., Kubo, A., Ito, E., Tange, Y., Tomioka, N., Saito, K., Nozawa, A., Funakoshi, K., 2004a. Thermal expansion of Mg_2SiO_4 ringwoodite at high pressure. Journal of Geophysical Research 109, 10.
Katsura, T., Yamada, H., Nishikawa, O., Song, M., Kubo, A., Shinmei, T., Yokoshi, S., Aizawa, Y., Yoshino, T., Walter, M.J., Ito, E., Funakoshi, K., 2004b. Olivine-wadsleyite transition in the system $(Mg, Fe)_2SiO_4$. Journal of Geophysical Research 109, 12.
Kohlstedt, D.L., Keppler, H., Rubie, D.C., 1996. Solubility of water in the alpha, beta and gamma phases of $(Mg, Fe)_2SiO_4$. Contributions to Mineralogy and Petrology 123, 345–357.
Leahy, G.M., Bercovici, D., 2007. On the dynamics of a hydrous melt layer above the transition zone. Journal of Geophysical Research 112, B07401, doi:10.1029/2006JB004631.
Litasov, K.D., Ohtani, E., Kagi, H., Jacobsen, S.D., Ghosh, S., 2007. Temperature dependence and mechanism of hydrogen incorporation in olivine at 12.5-14.0 GPa. Geophysical Research Letters 34, L16314, doi:10.1029/2007GL030737.
Matsukage, K.N., Jing, Z., Karato, S., 2005. Density of hydrous silicate melt at the conditions of Earth's deep upper mantle. Nature (London) 438, 488–491.
Murakami, M., Hirose, K., Yurimoto, H., Nakashima, S., Takafuji, N., 2002. Water in Earth's lower mantle. Science 295, 1885–1887.
Niu, F., Levander, A., Ham, S., Obayashi, M., 2005. Mapping the subducting Pacific slab beneath southwest Japan with Hi-net receiver functions. Earth Planet Science Letters 239, 9–17, doi:10.1016/j.epsl.2005.08.009.
Obayashi, M., Sugioka, H., Yoshimitsu, J., Fukao, Y., 2006. High temperature anomalies oceanward of subducting slabs at the 410-km discontinuity. Earth and Planetary Science Letters 243, 149–158.
Olbertz, D., Wortel, M.J.R., Hansen, U., 1997. Trench migration and subduction zone geometry. Geophysical Research Letters 24, 221–224.
Ohtani, E., Nagata, Y., Suzuki, A., Kato, T., 1995. Melting relations of peridotite and the density crossover in planetary mantles; chemical evolution of the mantle. Chemical Geology 120, 207–221.
Pino, N.A., Helmberger, D.V., 1997. Upper mantle compressional velocity structure beneath the West Mediterranean Basin. Journal of Geophysical Research, B, Solid Earth and Planets 102, 2953–2967.
Revenaugh, J., Jordan, T.H., 1989. A study of mantle layering beneath the western Pacific. Journal of Geophysical Research, B, Solid Earth and Planets 94, 5787–5813.
Revenaugh, J., Jordan, T.H., 1991a. Mantle layering from ScS reverberations; 1 waveform inversion of zeroth-order reverberations. Journal of Geophysical Research, B, Solid Earth and Planets 96, 19, 749–19,762.
Revenaugh, J., Jordan, T.H., 1991b. Mantle layering from ScS reverberations; 2 the transition zone. Journal of Geophysical Research, B, Solid Earth and Planets 96, 19,763–19,780.
Revenaugh, J., Jordan, T.H., 1991c. Mantle layering from ScS reverberations; 3 the upper mantle. Journal of Geophysical Research, B, Solid Earth and Planets 96, 19,781–19,810.
Revenaugh, J., Sipkin, S.A., 1994. Seismic evidence for silicate melt atop the 410-km mantle discontinuity. Nature (London) 369, 474–476.

Sakamaki, T., Suzuki, A., Ohtani, E., 2006. Stability of hydrous melt at the base of the Earth's upper mantle. Nature 439, 192–194.
Shieh, S.R., Mao, H., Hemley, R.J., Ming, L.C., 1998. Decomposition of phase D in the lower mantle and the fate of dense hydrous silicates in subducting slabs. Earth and Planetary Science Letters 159, 13–23.
Smyth, J.R., Frost, D., 2002. The effect of water on the 410-km discontinuity; an experimental study. Geophysical Research Letters 29, 4.
Smyth, J.R., Frost, D.J., Nestola, F., Holl, C.M., Bromiley, G., 2006. Olivine hydration in the deep upper mantle: effects of temperature and silica activity. Geophysical Research Letters 33, L15301, doi:10.1029/2006GL026194.
Song, T.R.A., Helmberger, D.V., Grand, S.P., 2004. Low-velocity zone atop the 410-km seismic discontinuity in the northwestern United States. Nature 427, 530–533.
Van der Hilst, R., Engdahl, E.R., Spakman, W., Nolet, G., 1991. Tomographic imaging of subducted lithosphere below northwest Pacific island arcs. Nature 353, 37–43.
Vinnik, L., Farra, V., 2002. Subcratonic low-velocity layer and flood basalts. Geophysical Research Letters 29, 4.
Vinnik, L., Kumar, M.R., Kind, R., Farra, V., 2003. Super-deep low-velocity layer beneath the Arabian Plate. Geophysical Research Letters 30, 4.
Vinnik, L., Farra, V., 2007. Low S velocity atop the 410-km discontinuity and mantle plumes. Earth and Planetary Science Letters, doi:10.1016/j.epsl.2007.07.051.
Walsh, J.B., 1969. New analysis of attenuation in partially melted rocks. Journal of Geophysical Research 74, 4333.
Wessel, P., Smith, W.H.F., 1998. New, improved version of the Generic Mapping Tools released. EOS Transactions of the American Geophysical Union 79, 579.
Wood, B.J., 1995. The effect of H_2O on the 410-kilometer seismic discontinuity. Science 268, 74–76.
Workman, R.K., Hart, S.R., 2005. Major and trace element composition of the depleted MORB mantle (DMM). Earth and Planetary Science Letters 231, 53–72.
Yoshino, T., Nishihara, Y., Karato, S.-I., 2007. Complete wetting of olivine grain boundaries by a hydrous melt near the mantle transition zone. Earth and Planetary Science Letters 256, 466–472.
Zhao, D., 2004. Global tomographic images of mantle plumes and subducting slabs: insight into deep Earth dynamics. Physics of The Earth and Planetary Interiors 146, 3–34.
Zhang, J., Herzberg, C., 1994. Melting experiments on anhydrous peridotite KLB-1 from 5.0 to 22.5 GPa. Journal of Geophysical Research 99, 17-17,742.